JOURNAL OF Materials CHEMISTRY

Optical properties and metal–insulator transitions in organic metals (BEDT-ATD)$_2$X(solvent) (X = PF_6, AsF_6, BF_4; solvent = THF, DHF, DO) [BEDT-ATD = 4,11-bis(4′,5′-ethylenedithio-1′,3′-dithiol-2′-ylidene)-4,11-dihydroanthra[2,3-*c*][1,2,5]thiadiazole]

Mikio Uruichi, Kyuya Yakushi* and Yoshiro Yamashita

Institute for Molecular Science, Myodaiji, Okazaki, 444-8585, Japan. Fax: 81-564-54-2254; E-mail: yakushi@ims.ac.jp

Received 11th April 2000, Accepted 5th September 2000
First published as an Advance Article on the web 26th October 2000

We present the polarized reflection spectra of (BEDT-ATD)$_2$X(solvent) (X = AsF_6, PF_6, BF_4; solvent = THF, DHF, DO), where THF is tetrahydrofuran, DHF 2,5-dihydrofuran, and DO 1,3-dioxolane. BEDT-ATD$^+$ has an intramolecular excitation in a very low-energy region (4000–5000 cm^{-1}). These isostructural compounds are characterized as strongly correlated quasi-1D metals. The optical spectra in all these compounds suggest that the screw-axis symmetry is broken below the metal–insulator transition temperature. This broken symmetry is confirmed by the X-ray diffraction experiment in (BEDT-ATD)$_2$$BF_4$(THF) and (BEDT-ATD)$_2$$PF_6$(DHF). The low-temperature structure has the $4k_F$-modulated lattice (dimerized structure). The magnetic susceptibility supports this $4k_F$ modulation as well. We present the low-temperature crystal structures of (BEDT-ATD)$_2$$BF_4$(THF) and (BEDT-ATD)$_2$$PF_6$(DHF). BF_4^- and THF are fully ordered in (BEDT-ATD)$_2$$BF_4$(THF) and DHF is almost ordered in (BEDT-ATD)$_2$$PF_6$(DHF). The vibronic modes are observed in the reflection spectra of all these compounds even above the metal–insulator transition temperature, which suggests that the screw-axis symmetry is locally broken.

Introduction

BEDT-ATD (4,11-bis(4′,5′-ethylenedithio-1′,3′-dithiol-2′-ylidene)-4,11-dihydroanthra[2,3-*c*][1,2,5]thiadiazole) is a recently synthesized butterfly-shaped molecule which shows a very small potential difference (90 mV) between the first and second oxidation potentials.[1,2] This potential difference is regarded as a measure of the on-site (on-molecule) Coulomb energy *U*. The small potential difference of BEDT-ATD resembles that of 4,9-bis(1,3-benzodithiol-2-ylidene)-4,9-dihydronaphtho[2,3-*c*][1,2,5]thiadiazole (BDNT), which involves a similar non-planar molecular skeleton.[3] We have previously reported the spectroscopic and solid-state properties of the 1 : 1 charge-transfer salts of BDNT with a focus on the reason of the very small potential difference (24 mV).[4–7] The origin of the small potential difference was ascribed to the large structural difference between BDNT$^+$ and BDNT^{2+} in solution.[7] However, the reason for the small potential difference of BEDT-ATD is not clear, since, unlike BDNT, BEDT-ATD yields only a 2 : 1 ratio of charge-transfer salts with the formal charge of +0.5, and thus there is presently no structural information on BEDT-ATD^{2+}. We speculate as follows: the more extended π-conjugation reduces the on-site Coulomb energy and thus reduces the potential difference without changing the geometry of BEDT-ATD^{2+}. This molecular property is advantageous for making an organic metal, despite the non-planarity of the molecule.

The 2 : 1 salts of BEDT-ATD occlude several kinds of organic solvents, and these salts are expressed as (BEDT-ATD)$_2$X(solvent). Hereafter we express the compound by the counter anion and the solvent as X(solvent). According to Imaeda *et al.*, these compounds are metallic near room temperature and show metal–insulator (MI) transitions at low temperature.[8] The MI transitions are detected by the electrical resistivity, thermopower, and spin susceptibility. Near the MI transition temperature, the compounds exhibit an upturn in resistivity and thermopower and a gradual decrease in the spin susceptibility. Among these compounds, PF_6(THF) and AsF_6(THF) (THF = tetrahydrofuran) show no anomaly in the spin susceptibility down to 3 K.[8] The thermopowers of these two compounds measured down to 50 K show no anomaly in this temperature range.[8] The electrical resistivity of these compounds behaves like that of a metal down to 200 K, but no lower-temperature resistivity has been reported due to the resistivity jumps.[9] Based on these results, Imaeda *et al.* claim that PF_6(THF) and AsF_6(THF) are metallic down to 3 K.[8] They calculate the tight-binding band and suggest a nearly closed two-dimensional Fermi surface.[10] We have reported the temperature-dependent reflectance of PF_6(THF),[11] and have found the following results: (1) PF_6(THF) has a quasi-one-dimensional (quasi-1D) band structure with a narrow bandwidth of 0.24 eV, and (2) the screw-axis symmetry begins to be broken below 100 K, which suggests the local lattice distortion. Imaeda *et al.* point out that the MI transition temperature depends upon the counter anions (X) and occluded organic solvents.[10] A very small structural perturbation such as high pressure, counter anion, or occluded solvent has an influence on the MI transition temperature. In the quasi-1D system, usually, the hydrostatic pressure or chemical pressure enhances the inter-chain interaction and thus suppresses the metal–insulator transition. In contrast, high pressure, smaller counter anion, and smaller organic solvent push up the MI transition temperature in (BEDT-ATD)$_2$X(solvent). This research aims to elucidate the mechanism controlling the MI transition. Imaeda *et al.* extended the number of compounds in this family by changing solvent molecules and counter anions and proposed the role of disorder of the solvent molecules in the MI transition.[10] In a previous paper,[11] we extended the reflectance measurement to all the compounds in this family, and conducted a low-temperature X-ray diffraction experiment to confirm the structural change. We will here discuss the disorder of the

 DOI: 10.1039/b002904l

solvent molecules and counter anions and the ordering mechanism of BF_4^- and THF in BF_4(THF).

Experimental

The crystals of BEDT-ATD salts with X^- anion were grown by electrochemical crystallization in tetrahydrofuran (THF), 2,5-dihydrofuran (DHF), and 1,3-dioxolane (DO) using the electrolytes *n*-Bu_4NX ($X = PF_6$, AsF_6, BF_4). All of the compounds are thin needle-like crystals, most developing along the *b*-axis, with development of the *bc* crystal face. The absorption spectrum in solution was measured on a HITACHI U-3500. A standard 10 mm-long cell was used for the measurement of the neutral BEDT-ATD molecule. A 1 mm-long cell was used for the measurement of BF_4(THF) to reduce the absorption by the solvent molecules in the near-infrared region. The polarized reflection spectrum was obtained using two spectrometers and a microscope (Spectratech IR-Plan). Nicolet Magna 760 FT-IR spectrometer was used for the 600–12000 cm^{-1} region and an Atago Macs320 multi-channel detection system was used for the 11000–30000 cm^{-1} region. For the low-temperature experiment, a small goniometer head was attached to the cold head of the cryostat (Oxford CF1104s) fixed on a XYZ stage. The details of the experimental method are as described previously.[11] The crystal face was determined by the X-ray diffraction method using a Rigaku AFC-7R-2 four-circle diffractometer. The X-ray diffraction experiment at low temperature was conducted using an imaging-plate detection system (Rigaku R-AXIS-4). The sample temperature was lowered by cold nitrogen. The temperature sensor was set at the nozzle 8 mm away from the sample. The static magnetic susceptibility was measured on a SQUID magnetometer(-Quantum Design MPMS-7). The diamagnetic susceptibility of BEDT-ATD was determined as 2.44×10^{-4} emu mol^{-1}. The diamagnetic susceptibilities of solvent molecules and counter anions were calculated using Pascal's law. The contribution of the diamagnetic susceptibilities were 6.07×10^{-4} emu mol^{-1} for PF_6(THF), 5.96×10^{-4} for PF_6(DHF), 6.00×10^{-4} for PF_6(DO), 6.12×10^{-4} for AsF_6(THF), and 5.79×10^{-4} for BF_4(THF).

Results and discussion

Band structure

Structural characteristics. Before discussing the optical and structural properties, let us briefly describe the molecular properties of BEDT-ATD. Fig. 1 shows the structural formula and the isosurface (the orbital contour value is 0.03) of the highest occupied molecular orbital (HOMO). The HOMO was calculated based on the optimized geometry – as obtained by the semi-empirical PM3 method – that yields the butterfly shape for BEDT-ATD. The structural formula shows that BEDT-ATD involves EDT (ethylenedithio-1,3-dithiole) rings, a half skeleton of BEDT-TTF. As shown in this figure, the HOMO is distributed in the EDT rings as well as in the central rings. The orbital in the EDT ring resembles that of BEDT-TTF's HOMO, where the probability of the electron is concentrated in the inner rings of the EDT groups. The HOMO of BEDT-ATD suggests that the π-conjugation is more extended than in BEDT-TTF.

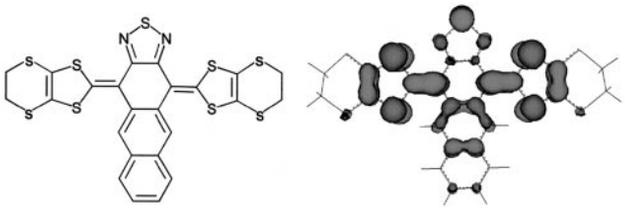

Fig. 1 Structural formula of BEDT-ATD and its highest occupied molecular orbital (HOMO).

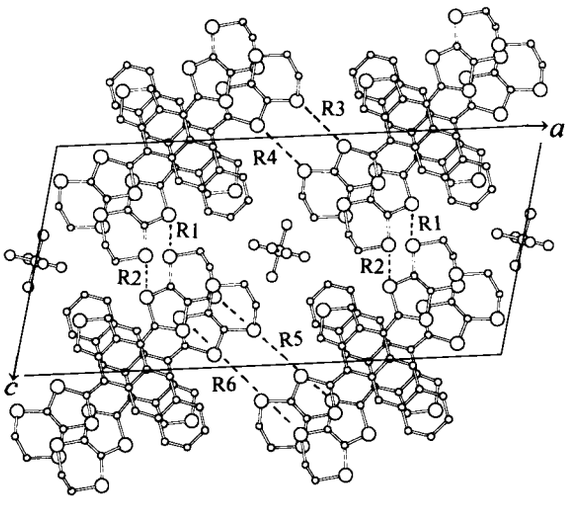

Fig. 2 Crystal structure of $(BEDT\text{-}ATD)_2PF_6$(solvent) viewed along the stacking axis. The orientationally disordered solvent molecule is not drawn in this figure. See the text for the inter-atomic distances, R1, R2, R3, R4, R5, and R6.

The crystals of $(BEDT\text{-}ATD)_2X$(solvent) ($X = PF_6$, AsF_6, BF_4; solvent = THF, DHF, DO) are isostructural with each other and belong to a monoclinic system with the space group of $P2_1/a$. The top view of the molecular arrangement is shown in Fig. 2. The unit cell consists of two molecular columns. Between these molecular columns, the solvent molecules are incorporated in the cavity surrounded by six BEDT-ATD molecules. The cavities are located at the positions (0,0,0) and (½, ½, 0). Since this cavity has the inversion symmetry, the asymmetric solvent molecules are orientationally disordered. As shown by the broken lines, R1 and R2, the molecular columns are linked with each other along the *c*-axis through S–S short contacts. The S–S short contacts comparable with the van der Waals distance (3.6 Å for S–S) are 3.67 Å for BF_4(THF), 3.65 Å for PF_6(DHF), 3.68 Å for PF_6(DO), 3.68 Å for AsF_6(THF), and 3.68 Å for PF_6(THF). No S–S contact shorter than the van der Waals distance is found in the direction of the *b*-axis. The intermolecular interaction along the *a*-axis is blocked off by the counter anions and solvent molecules. This crystal structure appears to form a two-dimensional conducting sheet parallel to the (100) plane. Fig. 3 shows a projection of this sheet onto the (100) plane. The repeating unit along the *b*-axis in each column consists of two BEDT-ATD molecules connected by the screw axis running along the *b*-axis.

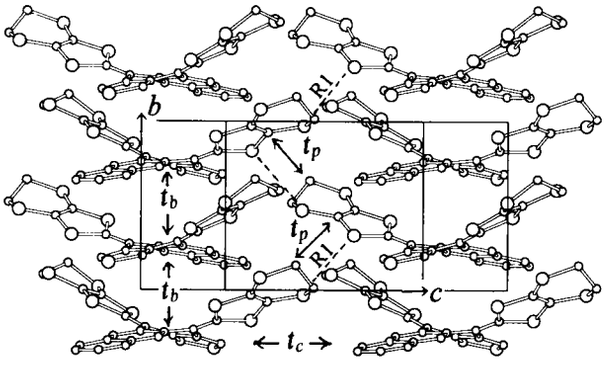

Fig. 3 Stacking pattern of BEDT-ATD projected onto the (100) plane and the definition of the transfer integrals, t_b, t_p, and t_c.

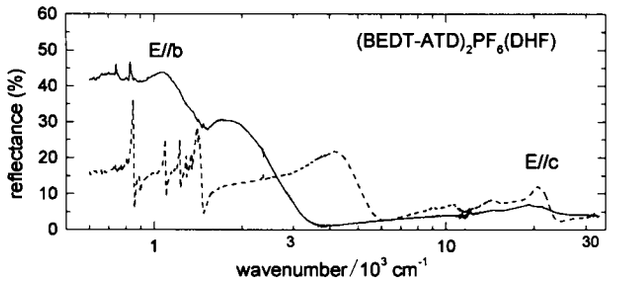

Fig. 4 Room-temperature polarized reflection spectrum of (BEDT-ATD)$_2$PF$_6$(DHF).

Room-temperature reflection spectra. Fig. 4 shows the polarized reflection spectrum of PF$_6$(DHF). All other compounds give essentially the same spectra. The reflectivity shows a large anisotropy when the light is polarized along the *b*- and *c*-axes in the conducting sheet. These compounds exhibit metallic resistivity along the *b*-axis (the stacking axis of BEDT-ATD). Taking the metallic behavior into account, the dispersion of the reflectivity in the infrared region of the E//*b* spectrum is ascribed to the intra-band optical transition. Along the *c*-axis, on the other hand, no electronic dispersion of the reflectivity is found down to 600 cm^{-1} in any of the compounds, although the short S–S contact (R1, R2) is found along the *c*-axis. This means the inter-column charge-transfer interaction is very weak, which is a reasonable conclusion when we look at the isosurface of the HOMO. The short S–S contact is found only between the inner and outer sulfurs of neighboring molecules, and the lobe of the outer sulfur is much smaller than that of the inner sulfur. Imaeda *et al.* calculate the transfer integrals as $t_b = -0.056$, $t_p = 0.016$, and $t_c = -0.0015$ eV using the relation $t = -10S$, where S is the overlap integral.[10] The definition of the transfer integrals is shown in Fig. 3. Based on these transfer integrals, they present a two-dimensional tight-binding band. However, it is clear according to the polarized reflection spectra shown in Fig. 4 that all of these compounds have quasi-1D bands.

Optical conductivity $\sigma(\omega)$ of (BEDT-ATD)$_2$PF$_6$(DHF)

Intramolecular excitation. Before moving on to the intermolecular excitation, we will describe the intramolecular electronic properties of BEDT-ATD. Fig. 5 shows the optical conductivity of PF$_6$(DHF) calculated *via* the Kramers–Kronig transformation and the solution spectra of the BEDT-ATD neutral molecule and (BEDT-ATD)$_2$PF$_6$(DHF) dissolved in CH_2Cl_2. From the comparison with solution spectra, the bands N1, N2, and N3 are assigned to the intramolecular electronic transition of the BEDT-ATD neutral molecule and C1, C2, C3, and C4 are assigned to those of the BEDT-ATD$^+$ cation radical. These optical transitions should be interpreted as inter-band transitions, but the above type of assignment is possible and convenient in this compound, since the bandwidth is very narrow compared with the excitation energies of inter-band transitions, as will be discussed in the next section. It should be noted that the intramolecular transition C1 of BEDT-ATD$^+$ is observed at 4.6×10^3 cm^{-1}, which is a very low excitation energy. This absorption band is assigned mainly to the optical transition from the second highest molecular orbital (a″) to the singly occupied HOMO (a′), the transition dipole of which is parallel to the direction connecting the two EDT groups. This assignment is consistent with the small angle of 34° between this direction and the *c*-axis. The corresponding intramolecular excitation is observed at 10000 cm^{-1} in BEDT-TTF salts. The very low excitation energy suggests that the π-conjugation is extended in this large molecule as shown in Fig. 1, although the molecule has a non-planar shape.

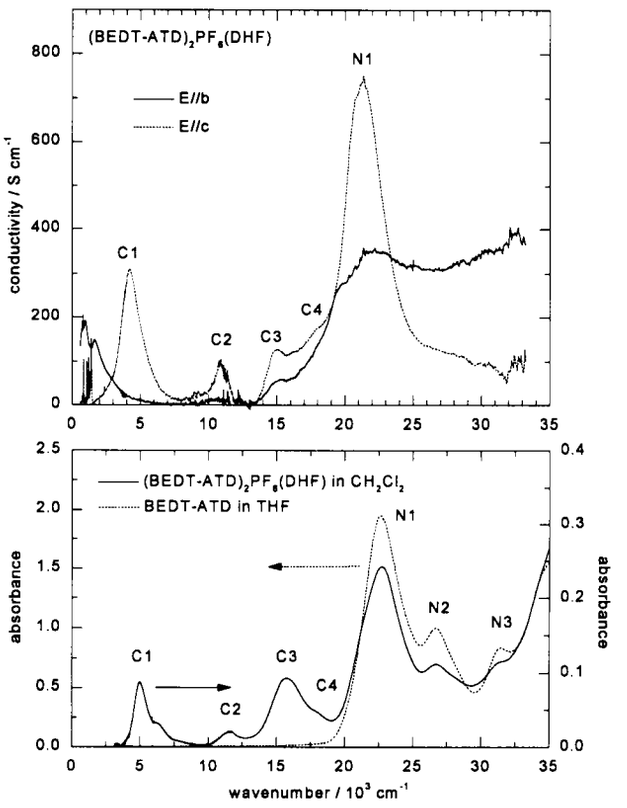

Fig. 5 Optical conductivity of PF$_6$(DHF) and solution spectra of BEDT-ATD^0 and BEDT-ATD$^+$.

Intermolecular excitation. Let us move on to the intra-band transition in the infrared region of the E//*b* spectrum. The intensity of the intra-band transition yields information on the bandwidth. The integrated intensity is connected with the plasma frequency by eqn. (1):[12]

$$\omega_p^2 = \frac{2}{\varepsilon_0 \pi} \int_0^{\omega_0} \sigma(\omega) \mathrm{d}\omega \tag{1}$$

where ε_0 is the permittivity of vacuum and ω_0 the cut-off frequency. To proceed with the numerical integration up to $\omega_0 = 5 \times 10^3$ cm^{-1}, we extrapolate $\sigma(\omega)$ linearly to $\sigma(0) = 30$ S cm^{-1} (dc conductivity at room temperature). The plasma frequency is calculated to be 3780 cm^{-1}. As we explained in the preceding section, a one-dimensional model is approximately applicable to this compound. We thus use eqn. (2) for a rough estimation of the transfer integral along the *b*-axis:[13]

$$t_b = \frac{\varepsilon_0}{2e^2} \frac{\pi(\hbar\omega_p)^2}{n_h b^2 \sin(\pi/4)} \tag{2}$$

where e is the electron charge, n_h the hole density, and b the lattice constant. The estimated transfer integral $t_b = 0.06$ eV is comparable with the value ($t_b = -0.056$ eV) calculated by Imaeda *et al.*[10] The bandwidth of the one-dimensional band ($= 4t_b$), 0.24 eV, is extremely narrow in comparison with those of other organic metals. This narrow band comes from the structural characteristics of the molecule: the overlap along the *b*-axis is hindered by the non-planar geometry of the molecule. As a matter of fact, there is no intermolecular S–S contact shorter than the van der Waals distance, even along the *b*-axis. It is surprising that such a narrow-band quasi-1D system yields a metal. Probably the narrow bandwidth is compensated by the small on-site Coulomb energy due to the large π-conjugation. The transfer integrals of other compounds seem to be nearly the same as that of PF$_6$(DHF).

As shown in the E//*b* spectrum of Fig. 5, the shape of the

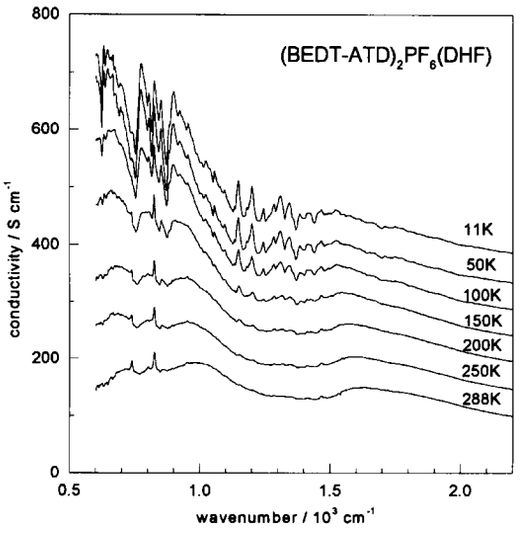

Fig. 6 Temperature dependence of the optical conductivity obtained by the Kramers–Kronig transformation of the reflectance of (BEDT-ATD)$_2$PF$_6$(DHF). Note the enhancement of the vibronic modes at low-temperature.

intra-band transition is not Drude-like in spite of the metallic transport properties. Contrary to the Drude response, the low-wavenumber side of room-temperature $\sigma(\omega)$ does not rise, but rather falls to the dc conductivity value $\sim 30\ \mathrm{S\ cm^{-1}}$, showing broad peaks around $1000\ \mathrm{cm^{-1}}$ and $1700\ \mathrm{cm^{-1}}$ (see also Fig. 6). The broad dip between these two peaks appears in the frequency region of the C=C stretching vibrational mode, which usually couples strongly with the CT state. Very similar dips are found in the same region in the metallic charge-transfer salts of tetramethyltetraselenafulvalene (TMTSF),[14] bis(ethylenedioxy)tetrathiafulvalene (BEDO-TTF),[15] and 2,5-bis(1,3-dithiol-2-ylidene)-1,3,4,6-tetrathiapentalene (BDT-TTP).[16] The origin of this dip structure is not clear at the moment, since this dip is not directly connected with the structural change or symmetry of the unit cell, in contrast to the vibronic modes that will be discussed in the next section. We suspect that the origin of this dip is related to the strong electron correlation.

Evolution of vibronic bands. Imaeda *et al.* reported that PF$_6$(DHF) shows a temperature-dependent resistivity with a continuous upturn at 150–200 K. This resistivity change suggests the second-order phase transition. As shown in Fig. 6, the E//*b* spectrum shows remarkably enhanced vibronic modes. The vibronic mode becomes quite visible below 100 K. The evolution of the many vibronic bands in the low-temperature spectrum has been explained by the electron molecular vibration (emv) coupling theory.[17] When the two molecules vibrate in *anti*-phase, the oscillatory dipole moment is induced between the molecules within the dimer *via* the charge-transfer interaction. The emv coupling theory was first formulated in a dimer[18] and then extended to the linear chain system.[17,19] Let us discuss the selection rule of the vibronic mode considering the unit cell dipole. The unit cell contains four BEDT-ATD molecules with the space group $P2_1/a$, which includes the factor group of C_{2h}. The symmetry of BEDT-ATD is C_s. When we consider the breathing mode with a' symmetry in the C_s point group, the four unit cell modes are classified as A_g, A_u, B_g, and B_u. As shown by the large hatched arrows in Fig. 7, the latter two modes induce a charge flow, and therefore an intermolecular dipole along the *b*-axis. The B_g mode is infrared inactive, since the induced dipoles cancel each other within the unit cell due to the inversion symmetry. The B_u mode produces a unit cell dipole along the *b*-axis, but the dipole in the same stack is cancelled out when we take account of the

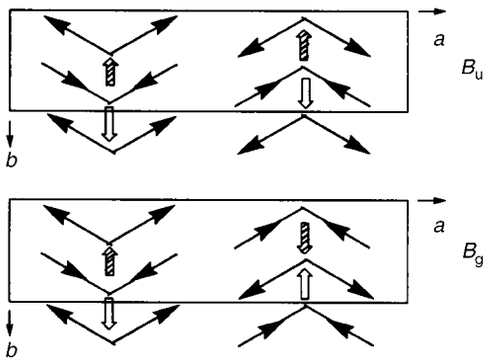

Fig. 7 Schematic drawing of the breathing mode of BEDT-ATD. The large arrows represent the charge flow coupled with the breathing modes. B_u mode becomes infrared active below the phase transition temperature.

induced dipole (open arrow) with the next unit cell.[20] When the screw-axis symmetry is broken ($P2_1/a \rightarrow Pa$), the hatched and open arrows become non-equivalent, and thus the B_u mode shows infrared activity along the *b*-axis. The intensity of a vibronic mode depends upon the displacement of the molecule from the position given by the symmetry. These modes are hardly observable at room temperature but begin to grow below 150 K. Fig. 6 demonstrates that the screw-axis symmetry is broken below 150 K. As in our previous study, the vibronic bands are already observable above the MI transition temperature in PF$_6$(THF).[11] This suggests that the screw-axis symmetry may be locally broken above the MI transition temperature in several compounds. The bottom panel of Fig. 8 shows the room-temperature E//*b* reflection spectra of five compounds in this family. The spectrum of PF$_6$(DO) already exhibits several vibronic modes (circles) at room temperature. This means PF$_6$(DO) involves a large structural fluctuation, although the MI transition temperature (100–150 K) is lower than that of PF$_6$(DHF) and BF$_4$(THF).

Structural change below the phase transition temperature

Lattice modulation. We have conducted a low-temperature X-ray diffraction experiment for PF$_6$(DHF) to confirm the

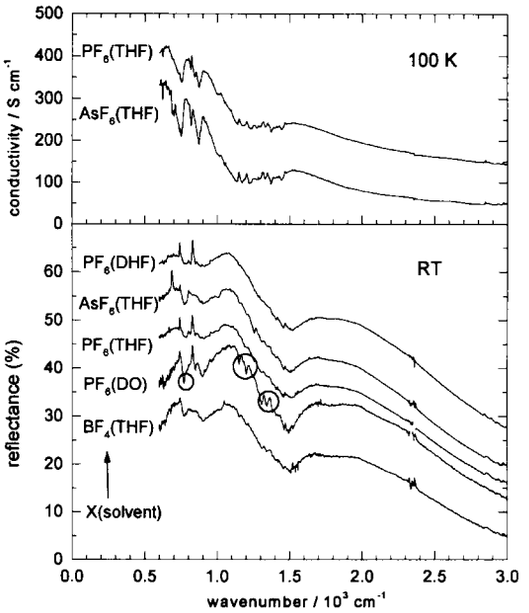

Fig. 8 Optical conductivity at 100 K of (BEDT-ATD)$_2$PF$_6$(THF) and (BEDT-ATD)$_2$AsF$_6$(THF) (top panel), and reflectance at room temperature of (BEDT-ATD)$_2$X(solvent). Note that the vibronic modes appear above the phase transition temperature.

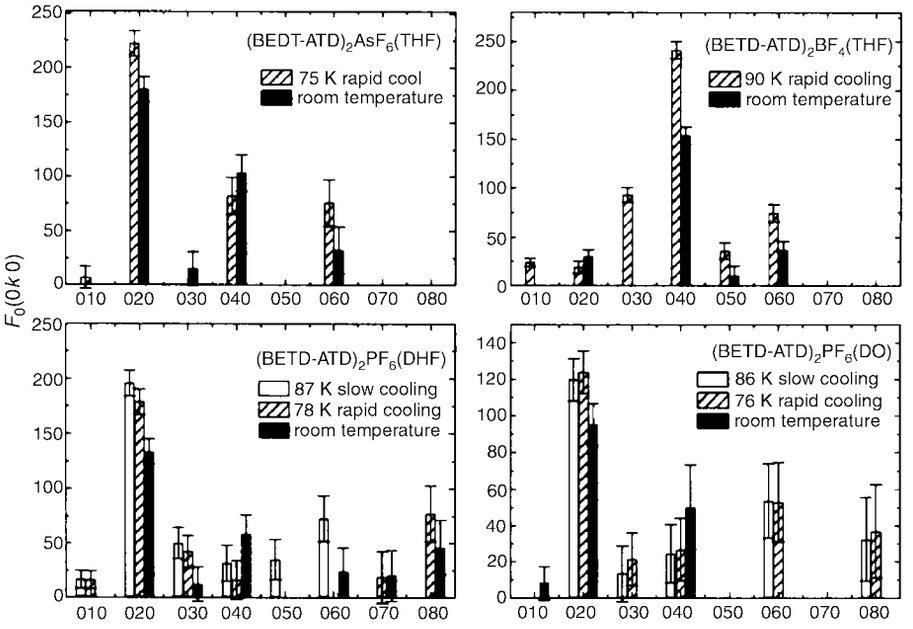

Fig. 9 Structure factors $|F_o|$ with $(0k0)$ indices of four BEDT-ATD salts at room and low temperatures. The error bar denotes $\pm 3\sigma(|F_o|)$.

change of unit-cell symmetry and to detect the possible super-structure. The main results are as follows. (1) We carefully searched for the reflection at $b^*/2$ in the oscillation photograph of the imaging plate, but found no streak or spot down to 87 K. (2) We determined the lattice parameters over each 50 K interval from 298 to 80 K, but we found no anomaly around the MI transition temperature. (3) At 87 K we also found no super-lattice along the *a*- and *c*-axes. We measured the intensity of reflection at 87 K two times using the same crystal, which was cooled slowly (0.5 K min^{-1}) the first time and rapidly (6–8 K min^{-1}) the second time. Based on our examination of the systematic absence of the $(h0l)$ reflections for $h=2n+1$, the glide-plane symmetry along the *a*-axis remains at this temperature in both cases. Identical results were obtained for PF_6(THF), AsF_6(THF), PF_6(DO), and BF_4(THF).

The results of the systematic absence of $(0k0)$ reflections at low temperature are shown in Fig. 9. The reflections, (030) and (050), of PF_6(DHF) appear weakly and significantly larger than $3\sigma(F_o)$. The appearance of the $(0k0)$ reflections with odd indices means that the screw-axis symmetry is broken. In BF_4(THF), the $(0k0)$ reflections of odd indices appear more strongly. This suggests the ordering of BF_4^- as well. On the other hand, in PF_6(DO), only the (030) reflection is slightly larger than 3σ (F_o) for the rapidly cooled crystal, and such a lack of systematic absence is found neither in AsF_6(THF) nor PF_6(THF). The existence of the systematic absence in the latter two compounds is consistent with their MI transition temperature ($T_{MI}<50$ K). As shown in the top panel of Fig. 8, however, the vibronic bands are already noticeable at this temperature in both compounds. Although the resistivity of PF_6(DO) shows a remarkable upturn around 100–150 K[21] and obviously suggests the structural fluctuation at room temperature (see Fig. 8, bottom panel), the systematic absence, which indicates the existence of the long-range order of symmetry, is almost maintained at 76 K.

Due to the screw-axis symmetry, we can take the effective periodic unit as $b'=b/2$.[22] Accordingly, the room-temperature phase has a 3/4-filled metallic band if the electron–electron interaction is negligible, but it has a half-filled metallic band in the strongly correlated limit. In PF_6(DHF) and BF_4(THF), the systematic absence of the $(0k0)$ reflections for $k=2n+1$is broken, while that of $(h0l)$ for $h=2n+1$ is maintained, and no super-structure is found. These low-temperature X-ray diffraction results indicate that the space group changes from $P2_1/a$ to *Pa* or *P2/a* below the MI transition temperature. In these space groups, the screw-axis symmetry is lost, so the periodic unit is doubled from $b/2$ to b and opens a gap at $k=\pm\pi/b$. This structural change corresponds to the $4k_F$ ($=b'^*/2=b^*$) lattice modulation (dimerization). The absence of the super-lattice with $b^*/2$ is supported by the static magnetic susceptibility, which is more sensitive to this kind of lattice modulation. The $2k_F$-lattice modulation forms a tetramer in the unit cell and

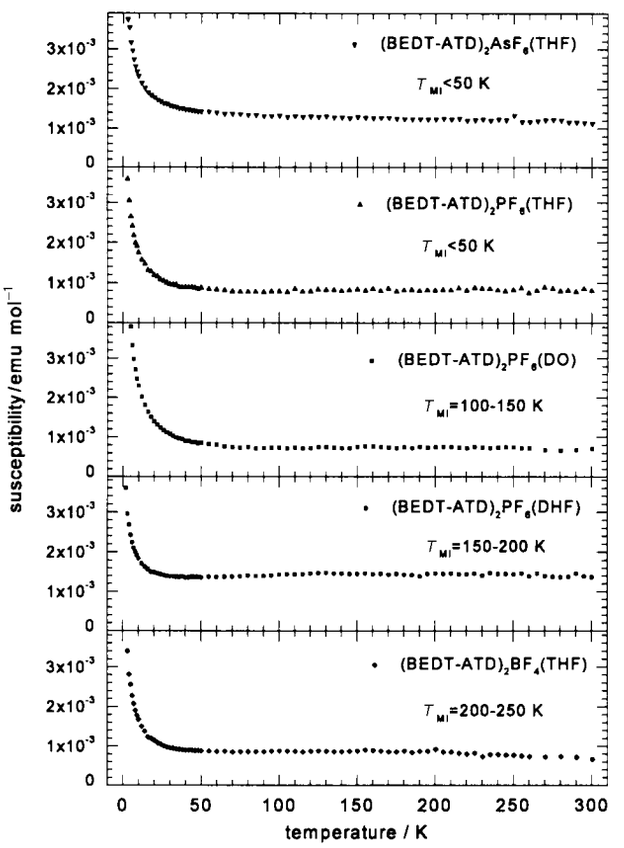

Fig. 10 Magnetic susceptibilities of BEDT-ATD salts. The susceptibility consists of almost temperature-independent paramagnetic component and a Curie component coming from impurity or crystal defect.

thus the two holes in the tetramer form a spin singlet. The $2k_F$-lattice modulation therefore brings about a non-magnetic state. In this case the paramagnetic susceptibility should vanish to 0 K below the MI transition temperature. As shown in Fig. 10, however, the paramagnetic susceptibility is almost temperature-independent and does not show such a tendency.[23] We therefore conclude that the insulating phase has a $4k_F$-modulated lattice. This structural change is consistent with the strong correlation in these compounds suggested by the reflection spectra. Finally, the strong correlation is also suggested by the high paramagnetic susceptibility, which is slightly higher than the value ($(0.5–0.6)\times10^{-3}$ emu mol^{-1}) of the highly correlated quasi-1D conductor $(TMTTF)_2X$,[24] and almost comparable with the value (1×10^{-3} emu mol^{-1}) of quasi-1D Mott insulators β′-$(BEDT\text{-}TTF)_2X$ (X = ICl_2, $AuCl_2$).[25]

Low-temperature crystal structure. As we described in the preceding section, the space group changes from $P2_1/a$ to $P2/a$ or Pa in PF_6(DHF) and BF_4(THF). Since $P2/a$ requires an orientational disorder for BEDT-ATD, we selected the space group Pa and solved the structure using slowly cooled crystals. For the other three compounds we solved the crystal structures taking $P2_1/a$. If we take the space group as Pa, the center of symmetry is lost, and thus the orientationally disordered DHF and THF should be ferroelectrically ordered along the b axis. The orientationally disordered BF_4 is also ordered in BF_4(THF) in this space group. In fact, neither inverted BF_4 nor THF was recognized in the difference synthesis map. However, the inverted DHF was slightly recognized in the residual map of PF_6(DHF). This result means that disordered BF_4 and THF are fully ordered at 90 K in BF_4(THF) (T_{MI} = 200–250 K), but DHF in PF_6(DHF) (T_{MI} = 150–200 K) is still slightly disordered at 87 K. DO in PF_6(DO) is almost disordered at 86 K, although the MI transition occurs at 100–150 K.[26] The THF in AsF_6(THF) ($T_{MI}<50$ K) and PF_6(THF) ($T_{MI}<50$ K) are disordered at 75 K and 100 K, respectively. Therefore the ordering of solvent molecules and anions is likely to be correlated with the MI transition temperature.

We will next examine the structural change after the screw-axis symmetry is broken. The S–S contacts (R1 and R2) between the adjacent molecular columns run along the screw axis as if "sewing" the two columns together (see Figs. 2 and 3). The contacts R1 and R2 are equivalent to each other due to the screw-axis symmetry in metallic phase. They are shortened at low temperature, and the deviation from the screw-axis symmetry is largest in BF_4(THF).[27] On the other hand, the deviation is very small in PF_6(DHF), although the space group changes from $P2_1/a$ to Pa. The environment around the solvent molecule loses the inversion symmetry as well. This structural change is expressed by the equivalent S–S distances R3, R4 and R5, R6 (see Fig. 2). R3 and R4 are above and below the solvent molecule capping the cavity, while R5 and R6 are at the same solvent-molecule level. Also in this case the deviation from the inversion symmetry is largest in BF_4(THF).[27] The ordering of BF_4 seems to contribute to this large structural change of BEDT-ATD.

Phase transition and disorder of solvent molecules. Below the MI transition temperature, the solvent molecules are fully ordered in BF_4(THF), still slightly disordered in PF_6(DHF), and almost disordered in PF_6(DO). To examine the possibility of the order–disorder transition in BF_4(THF), we estimate the Coulomb energy between BF_4^- and dipole–dipole interaction between solvent molecules. The electrostatic energy between the nearest neighbor BF_4^- $(0,0,\frac{1}{2})$ and $(0,1,\frac{1}{2})$ is 0.9068 and 0.9178 eV for the antiferroelectric and ferroelectric configurations, respectively. The dipole–dipole interaction between the nearest neighbor THF (0,0,0) and (0,1,0) is −0.0027 and 0.0025 eV for the antiferroelectric and ferroelectric configurations, respectively. In both cases the antiferroelectric configuration is more stable than the ferroelectric configuration, in contrast to the ordered structure in the low-temperature phase. The differences between the two configurations are 0.011 eV (= 128 K) for BF_4^- and 0.0052 eV (= 60 K) for THF. For this calculation, we estimate the point charge on each atom of BF_4^- and THF using the semi-empirical PM3 method.[28] This difference is comparable with the MI transition temperature (200–250 K) of BF_4(THF). The orientation of BF_4^- and THF appears to compete with the $4k_F$-lattice modulation.

To examine the optimum orientation of BF_4^- and THF required by the electrostatic force between them, we have calculated the difference of electrostatic energy between two hypothetical arrangements, models A and B in Fig. 11. A is the actual low-temperature structure, while B is the hypothetical structure with an antiferroelectric arrangement along the b-axis. The structure B requires the doubling of the periodic unit along the b-axis. In both models, we preserve the glide plane symmetry, and replace BEDT-ATD by point charges of +0.5. We calculate the infinite sum of the electrostatic energy between these point charges using the Ewald method.[29] The lattice sums per $(BEDT\text{-}ATD)_2BF_4$(THF) are −1.0869 eV for model A and −1.0877 eV for model B. The difference is only 0.8 meV (= 1 K), which is much smaller than the MI transition temperature. This calculation means that A and B are almost degenerate in energy, so we suppose that the orientation of BF_4^- and THF in the insulating phase is determined by the asymmetric environment of the cavity produced by the structural change of BEDT-ATD. Therefore, the ordering of BF_4^- and THF just accompanies the $4k_F$ structural change caused by the instability of the BEDT-ATD column. The ordering of BF_4^- and THF may occur *via* the second-order phase transition as well as the MI transition. The possibility of an order–disorder phase transition of solvent molecules in the other 4 compounds is much less than that in BF_4(THF), since the counter anions PF_6^- and AsF_6^- have a center of symmetry and the dipole–dipole interaction is much smaller than the repulsive interaction between anions. We speculate that the solvent molecules may freeze into glass states at low temperature in PF_6(THF), AsF_6(THF), PF_6(DO), and PF_6(DHF). We have conducted a preliminary experiment of the heat capacity of BF_4(THF). If BF_4^- and/or THF shows the first-order phase transition of an order–disorder type, we should observe an anomaly in heat capacity due to the entropy change $nRT\ln 2$ (n = 1 or 2). We could not detect such an

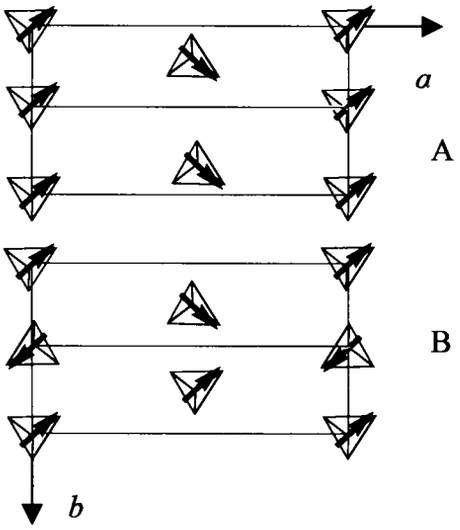

Fig. 11 Schematic arrangement of BF_4^- (tetrahedron) and DHF (arrow) in the doubled unit cell.

anomaly within the experimental error. The temperature dependence of the permittivity of vaccum and high-resolution solid NMR experiment should provide a wealth of information on the ordering and motion of the solvent molecules and BF_4^-.

If the solvent molecules are ordered antiferroelectrically, this ordering would break the inversion symmetry and thereby promote the $2k_F$-lattice distortion (tetramerization) of BEDT-ATD. However, the above discussion suggests that the structural phase transition is not triggered by the order–disorder transition of solvent molecules and/or BF_4^- but by the $4k_F$-lattice instability inherent in a strongly correlated quasi-1D system. The solvent molecules do not positively contribute to the phase transition, but rather just follow the $4k_F$-lattice distortion (dimerization). In PF_6(DO), for example, the solvent molecules seem to remain disordered at 76 K. The phase transition temperature is determined by the balance between the energy gain of the kinetic energy of charge carriers and the energy cost to distort the lattice. Thus the role of the solvent molecules is simply to tune the transfer integral along the stacking axis, resulting in the observed energy gain.

Conclusion

$(BEDT\text{-}ATD)_2X$(solvent) ($X = PF_6$, BF_4; solvent = THF, DHF, DO) is a narrow-band quasi-1D metal with strong correlation. The X-ray diffraction experiment confirmed the change of the space group at around 90 K in BF_4(THF) and PF_6(DHF) salts. According to the low-temperature reflection spectra, however, all these compounds show structural change or fluctuation that breaks the screw-axis symmetry. The MI transition of this system is considered to be the Peierls–Hubbard-type phase transition with $4k_F$ modulation, which transition is characteristic in a strongly correlated quasi-1D system. This mechanism is the driving force of this structural phase transition, and the ordering of BF_4^- and solvent molecules in BF_4(THF) and PF_6(DHF) simply follows this structural change.

Acknowledgements

This research was supported in part by a Grant-in-Aid for Scientific Research on Priority Areas (B) of Molecular Conductors and Magnets (Area No. 730/Grant No. 11224212) from the Ministry of Education, Science, Sports and Culture of Japan.

References

1 Y. Yamashita, S. Tomura and K. Imaeda, *Synth. Met.*, 1995, **71**, 1965.
2 Y. Yamashita, M. Tomura, S. Tanaka and K. Imaeda, *Synth. Met.*, 1997, **86**, 1795.
3 Y. Yamashita, K. Ono, S. Tanaka, K. Imaeda and H. Inokuchi, *Adv. Mater. (Weinheim Ger.)*, 1994, 295.
4 J. Dong, K. Yakushi and Y. Yamashita, *J. Mater. Chem.*, 1995, **5**, 1735.
5 V. N. Denisov, A. N. Ivlev, B. N. Mavrin, K. Yakushi, J. Dong and Y. Yamashita, *Chem. Phys. Lett.*, 1995, **246**, 176.
6 J. Dong, K. Yakushi, Y. Yamashita, K. Imaeda and H. Inokuchi, *Phys. Status Solidi B*, 1996, **95**, 611.
7 K. Yakushi, J. Dong, M. Uruichi and Y. Yamashita, *Mol. Cryst. Liq. Cryst.*, 1996, **284**, 223.
8 K. Imaeda, Y. Yamashita, S. Tanaka and H. Inokuchi, *Synth. Met.*, 1995, **73**, 107.
9 According to our resistivity measurement, the resistivity smoothly decreased down to 160 K and then showed multiple resistivity jumps below this temperature.
10 K. Imaeda, J. Krober, C. Nakano, M. Tomura, S. Tanaka, Y. Yamashita, H. Kobayashi, H. Inokuchi and A. Kobayashi, *Mol. Cryst. Liq. Cryst.*, 1997, **296**, 205.
11 M. Uruichi, K. Yakushi and Y. Yamashita, *J. Phys. Soc. Jpn.*, 1999, **68**, 531.
12 C. S. Jacobsen, *Low-Dimensional Conductors and Superconductors*, ed. by D. Jerome and L. G. Carson, Plenum, New York, 1986, p. 284.
13 J. B. Torrance, B. A. Scott, B. Welber, F. B. Kaufman and P. E. Seiden, *Phys. Rev. B Condens. Matter*, 1979, **19**, 730.
14 D. Pedron, R. Bozio, M. Mneghetti and C. Pecile, *Phys. Rev. B Condens. Matter*, 1994, **49**(II), 108393.
15 J. Ulanski, K. Yakushi, H. Yamochi and G. Saito, *J. Phys.: Condens. Matter*, in preparation.
16 J. Ouyang, K. Yakshi, Y. Misaki and K. Tanaka, *J. Phys. Soc. Jpn.*, 1998, **67**, 3191.
17 R. Bozio, M. Meneghetti and C. Pecile, *Phys. Rev. B Condens. Matter*, 1987, **36**(II), 7795.
18 M. J. Rice, N. O. Lipari and S. Strässler, *Phys. Rev. Lett.*, 1977, **39**, 1359; M. J. Rice, *Solid State Commun.*, 1979, **31**, 93.
19 H. J. Schulz, *Phys. Rev. B Condens. Matter*, 1978, **18**, 5756.
20 If the induced dipole is largely tilted, that is, the center of the molecule is largely shifted from the screw axis, the vibronic modes will appear in the (100) plane.
21 K. Imaeda, private communication.
22 V. Heine *Group Theory in Quantum Mechanics*, Pergamon, Oxford, 1960, p. 284.
23 The magnetic susceptibility shows no anomaly at the MI transition temperature. This kind of spin and charge separation is commonly observed in a highly correlated quasi-1D system.
24 C. Coulon, P. Delhaes, S. Flandrois, R. Lagnier, E. Bonjour and J. M. Fabre, *J. Phys.*, 1982, **43**, 1059.
25 N. Yoneyama, A. Miyazaki, T. Enoki and G. Saito, *Bull. Chem. Soc. Jpn.*, 1999, **72**, 639.
26 We have solved the low-temperature crystal structure of PF_6(DO) using the space group of $P2_1/a$, since the deviation from the systematic absence is very small. However, we believe the screw-axis symmetry is broken in this compound as well, because very large vibronic band appears at low temperature. So the MI transition of this compound can be ascribed to the $4k_F$ lattice modulation as well.
27 Crystallographic files in .cif format (CCDC reference number 1145/259), lattice parameters and S–S distances are available as supplementary data. For direct electronic access see http://www.rsc.org/suppdata/jm/b0/b002904l/
28 The dipole moment of THF calculated by the PM3 method is 1.68 D, which agrees very well with the experimental value 1.71 D. The point charges thus obtained are 0.3730 for B, −0.3430 for F, −0.2720 for O, and 0.0680 for CH.
29 R. M. Metzger, *J. Chem. Phys.*, 1972, **57**, 1870.